



Article

Aerodynamic Analysis of a Wind-Turbine Rotor Affected by Pitch Unbalance

Francesco Castellani ^{1,*}, Abdelgalil Eltayesh ², Matteo Becchetti ¹ and Antonio Segalini ³

¹ Department of Engineering, University of Perugia, via G. Duranti 93, 06125 Perugia, Italy; matteobecchetti@alice.it

² Mechanical Engineering Department, Benha Faculty of Engineering, Benha University, Benha 13512, Egypt; abdelgalil.youssef@bhit.bu.edu.eg

³ KTH Royal Institute of Technology, FLOW, STandUP for Wind, Osquars Backe 18, 10044 Stockholm, Sweden; segalini@mech.kth.se

* Correspondence: francesco.castellani@unipg.it; Tel.: +39-075-585-3709

Abstract: The aerodynamics of a rotor with pitch imbalance has been investigated experimentally and numerically in the present work. The comparison of mean velocity and turbulence intensity in the balanced and unbalanced cases indicated that a pitch imbalance modifies both the mean velocity and the turbulent activity; the latter is weakly increased by the imbalance. Spectral analysis indicated that the dynamics of the wake is also affected by the pitch imbalance since the tip vortices lose strength and disorganise more quickly than in the balanced case. The pitch imbalance has, however, a detrimental effect on the power coefficient and it affects the thrust coefficient as well. Only the blade affected by the imbalance shows significant modifications of the applied load, while the other blades operate with the same loading conditions.

Keywords: rotor aerodynamics; pitch imbalance; wind-tunnel test; CFD



Citation: Castellani, F.; Eltayesh, A.; Becchetti, M.; Segalini, A. Aerodynamic Analysis of A Wind-Turbine Rotor Affected by Pitch Unbalance. *Energies* **2021**, *14*, 745. <https://doi.org/10.3390/en14030745>

Academic Editor: Fausto Pedro García Márquez
Received: 30 December 2020
Accepted: 26 January 2021
Published: 31 January 2021

Publisher's Note: MDPI stays neutral with regard to jurisdictional claims in published maps and institutional affiliations.



Copyright: © 2021 by the authors. Licensee MDPI, Basel, Switzerland. This article is an open access article distributed under the terms and conditions of the Creative Commons Attribution (CC BY) license (<https://creativecommons.org/licenses/by/4.0/>).

1. Introduction

With the strong development of wind technology, the aerodynamic performance of wind rotors is reaching the edges of the current understanding of turbine aerodynamics, especially for large horizontal-axis wind turbines (HAWT). The industrial and the scientific communities are strongly involved in research and development activities aimed at further improving the performances of new turbines as well as boosting the production of operating units [1,2]. The aerodynamic design optimisation involves not only the single machines but also the whole wind farm: since turbine wakes interact significantly in a large farm, deep knowledge of the wake structure and dynamics is fundamental in order to develop new farm control strategies to maximise the farm's performance even with a lower efficiency for the single units.

Often the actual operation of wind turbines can be affected by installation issues so that the performance and the aerodynamic behaviour of the rotor can be different than what is expected, introducing undesirable loads. The most common issues are yaw misalignment [3–5] and pitch unbalance: while the effect of the former is a topic widely investigated in the study of farm-control strategies, the aerodynamics of a rotor affected by pitch unbalance is a topic poorly covered by the scientific literature. Most of the existing literature on pitch unbalance focuses on loads and control [6–8], but the wake aerodynamics with an unbalanced blade has not been deeply investigated. An exception is the work of Oggiano et al. [9] who studied experimentally and numerically the effects of unbalancing one blade on the HAWT performance: in this study one blade was pitched by 20° and the effect was analysed at several tip-speed ratios. This study identified a noticeable loss in power coefficient, as one blade was mostly stalled with a dramatic increase in its drag, affecting directly the power coefficient. 20° pitch change is sufficiently large to achieve a

non-negligible perturbation amplitude with respect to the balanced case and severe stall is expected along the blade. The question that remains is how a small change in pitch affects the near-wake evolution and dynamics. This quest motivates the present work which is aimed at the flow characterisation of the wind-turbine wake (both numerical and experimental) in the presence of a small pitch imbalance.

The manuscript is structured as follows. Section 2 reports details about the experimental campaign, while the simulation setup is described in Section 3. The results are first described in terms of mean velocity deficit and turbulence intensity in Section 4, together with some experimental results about the coherent structures detected with a spectral analysis. A load analysis is also performed by means of the pressure-coefficient distribution from the numerical simulations. A discussion of the results is done in Section 5 with some final considerations.

2. The Experimental Analysis

The experimental work was performed in the “R. Balli” wind tunnel of the University of Perugia (Italy); the tunnel is characterised by closed-loop configuration and an open test section (as shown in Figure 1), and the wind flow is generated by means of a fan driven by a 375 kW electric motor. The inlet section has an area of 5 m², whereas the recovery-section area is 7 m². The inflow conditions in the inlet section are measured with two Pitot-static tubes and a cup anemometer placed near the outlet of the converging section, just upstream of the test section. All the atmospheric parameters (static air pressure, temperature and relative humidity) are collected on a station point in the testing room. A honeycomb upstream of the test section is used to reduce the inflow turbulence in the test section.

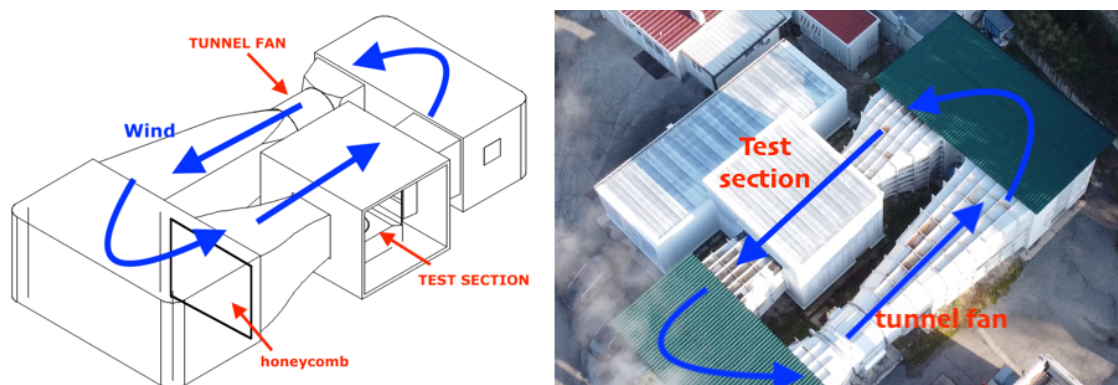


Figure 1. Schematic representation of the wind tunnel “R. Balli” at the University of Perugia.

The velocity field behind the scaled wind turbine model was investigated through a traversing system with a two-axis table moving a rake composed by a hot-wire anemometer and a Prandtl probe; in this way it was possible to investigate the wind velocity on a plane orthogonal to the wind direction in the test section and to calibrate the hot-wire probe when needed. Movements on both axes are driven by high-quality stepper motors: encoders are used to get the feedback of the position while ensuring high precision in the displacements with resolution of 0.01 mm for both axes. The horizontal axis uses a belt system to move the tower, wherein the vertical guide is mounted by using a worm screw to move the probe support.

A Dantec streamline 90N10 was used for the hot-wire measurements to handle a single-wire probe Dantec 55P11. The signals were sampled during 10 s for each measurement point with a sampling frequency of 10 kHz. This corresponds to a 95% confidence interval of the order of 0.6% in velocity due to statistical convergence. The hot-wire probe was calibrated in-situ against the Prandtl tube with the turbine braked and outside the wake of the rotor. The systematic error of the pressure transducer was 1.6%, corresponding to a maximum error in velocity of 0.8%. A thermocouple was also used to monitor the ambient temperature during calibration and perform temperature corrections of the hot-wire signal

during measurements. The analogue outputs of the probes were acquired using a cDAQ chassis 9185 and a 9211 module for the ADC conversion with a sampling rate of 100 kHz, i.e., much faster than the sampling frequency used for the hot-wire probe.

The horizontal-axis wind turbine model under test was designed with the same rotor geometry of the model tested in the past at NTNU [10]. The length scale was reduced by a factor two in order to have a decrease in the confinement effect [11] with respect to the NTNU experiments (here the blockage ratio is 2.5%, thus requiring no blockage corrections). This gave the possibility to compare the present results with other obtained at a larger Reynolds number with a significantly higher blockage. It is worth to mention that, while the rotor was a downscaled version of the NTNU turbine, both the nacelle and the tower were not the same as they were designed independently.

Figure 2 shows the layout of the measurement campaign with the model and the traversing system placed downstream in order to characterise the near wake. The traversing system was fixed to the ground while the turbine was moved upstream or downstream in order to characterise several streamwise stations (relative to the rotor axial location).

Half of the experiments were done with a balanced rotor, similar to the NTNU configuration [10]. The unbalanced experiments were conducted with only one turbine blade unbalanced by 5° upwind with respect to the others. The measurements were carried out at the inlet velocity of $U_{ref} = 5.4$ m/s, a turbulence intensity of 1% and a turbine rotational speed of 152 rad/s, which is equivalent to a tip speed ratio (TSR) of 6.3, i.e., typical of existing utility-scale HAWT.



Figure 2. Photo showing the test layout.

3. The Numerical Model

Numerical simulations have been carried out by using the commercial computational fluid dynamics (CFD) package Ansys Fluent 18.1 [12]. The numerical simulations were performed to understand the effect of wind turbine unbalance on the performance of HAWT (i.e., the power coefficient, C_P , and thrust coefficient, C_T) as well as on the flow field behind the turbine rotor by solving the unsteady incompressible Reynolds-averaged Navier–Stokes (URANS) equations. The semi-implicit method for pressure-linked equation (SIMPLE) was used to solve the discretised equations. The discretisation scheme used in numerical calculations was an upwind differencing scheme. It was chosen to use first-order upwind discretization for the initial part of the solution to help the convergence, while then it was set to second-order upwind to obtain a higher accuracy.

According to Bardina et al. [13], who compared the performance of different turbulence models, the SST $k-\omega$ model can predict the flows with strong adverse pressure

gradients where separation occurs. The SST $k-\omega$ is an empirical model based on modelled transport equations for the turbulence kinetic energy, k , and the specific dissipation rate, ω [14]. Several researchers have also obtained a good agreement between experimental measurements and numerical calculations using the SST $k-\omega$ turbulence model [15–17]. Therefore, this model was employed in the present work to account for the turbulent flow.

The computational domain was divided into an inner and an outer volume: the outer volume was defined as a stationary domain while the inner volume was defined in the non-inertial reference frame rotating with the turbine blades. A sliding moving mesh was imposed at the interface between inner and outer volumes. Figure 3 illustrates the computational domain and the associated boundary conditions. The preprocessor Gambit (release 2.3.16) [18] was used to generate the computational domain and the mesh for the HAWT. The turbine rotor and hub were the only simulated parts in this study, as shown in Figure 4. Other parts of the wind turbine such as the nacelle and the tower were not included.

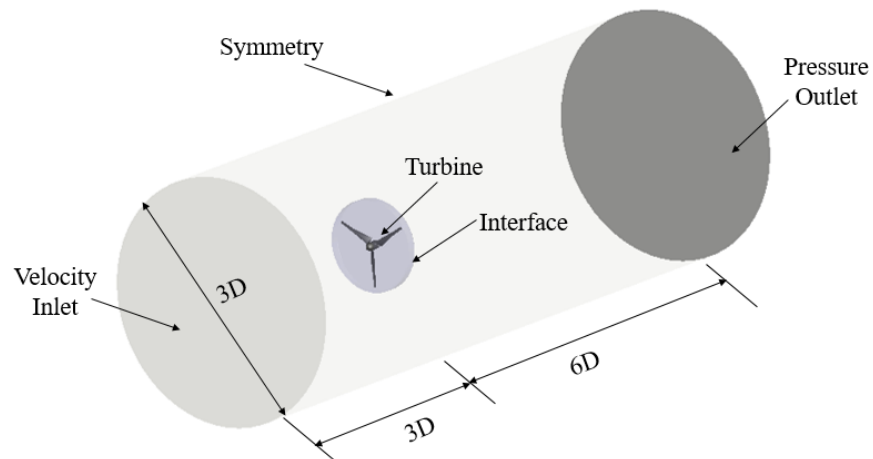


Figure 3. Computational domain and boundary conditions.

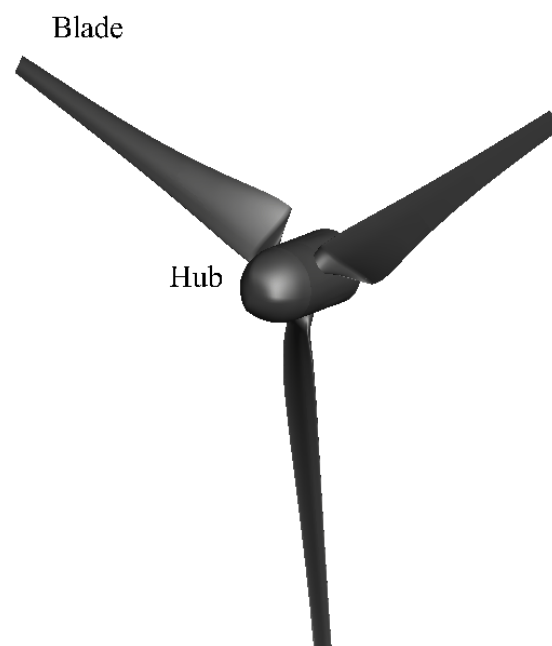


Figure 4. Geometry of the turbine blade.

The computational domain was composed by a cylinder with a diameter of three times the turbine diameter, D . Concerning the dimensions of the computational domain, previous studies analysed the effect of computational domain size and they obtained acceptable results: for instance, Lee et al. [17] placed the domain inlet at $0.75D$ upstream while the outlet domain at $5D$ downstream the turbine, whereas Van Rooij and Arens [19] used a downstream length of $3D$. Following these authors, in this paper the computational domain extended $3D$ in the upstream and radial directions and $6D$ downstream of the rotor.

For the balanced and unbalanced case the whole turbine rotor was simulated without exploiting the angular periodicity of 120° to ensure the same setup in both cases. The turbine blade twist and taper made the grid generation difficult with a single block. Therefore, the grid was generated in a multi-block topology with hybrid types of cells. The domain was divided into 189 blocks for the rotating zone and 94 blocks for the stationary zone, where the grid was generated in each block individually. Moshfeghi et al. [20] investigated different inflation layers spacing on the performance of the National Renewable Energy Laboratory (NREL) Phase VI HAWT. They showed that 12–20 nodes were required inside the boundary layer for acceptable results. A similar distribution was used by Eltayesh et al. [21] in their study to assess the effect of tunnel blockage on wind turbine performance, and thereby the same distribution of inflated layers will be adopted here too. The turbine blade has here a sharp trailing edge: to overcome this problem, the blocks close to the blade were generated using a structured H-grid [15]. This type of mesh allowed for a fine grid near the solid walls to resolve the flow within the boundary layer over the blade as shown in Figure 5.

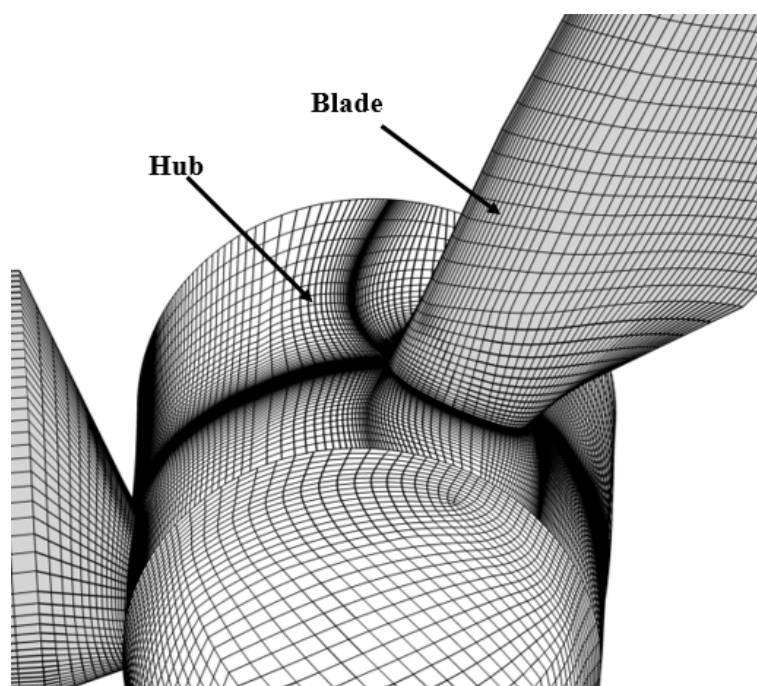


Figure 5. Detail of the hub and blade surface mesh.

The blocks representing the inlet and outlet regions were structured while the block near the hub nose region employed an unstructured grid. The surface of the blade was meshed with 132 cells in the chord-wise direction: the cells were concentrated at the leading and trailing edge, while 162 cells were distributed in the span-wise direction. Since a thin boundary layer is present near the blade, a grid refinement was added in the normal direction: the inflation layer had 16 rows, where the first row height was 0.01 mm from the blade wall and the growth factor of the grid was 1.25. This leads to a y^+ on the pressure side, suction side and tip of the blade of less than 4 and increases at the nose region to about 6, as illustrated in Figure 6.

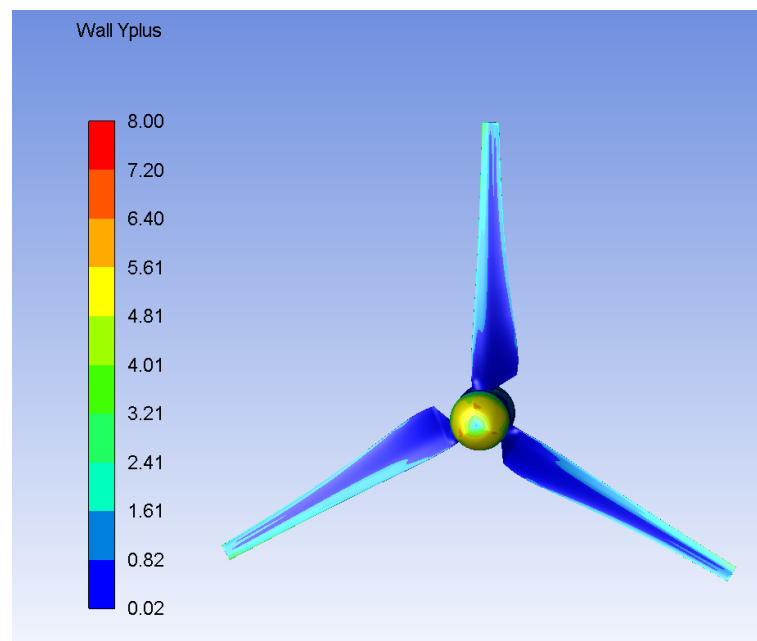


Figure 6. Contour of the wall y^+ .

Three different grids with 5.47, 6.93 and 8.1 million cells were used for the balanced-rotor case to study the grid-convergence sensitivity on the turbine performance, as shown in Figure 7. As visible from the figure, the sensitivity of the power coefficient is reasonably small to consider the present results converged. Therefore, the final mesh contained about 5.35 million cells for the rotating zone while the stationary zone comprised about 2.75 million cells, for a total of 8.1 million cells. Figure 8 shows the final computational mesh for the entire domain. The mesh has a maximum aspect ratio of 343 and 1260 for the rotating and fixed zone, respectively.

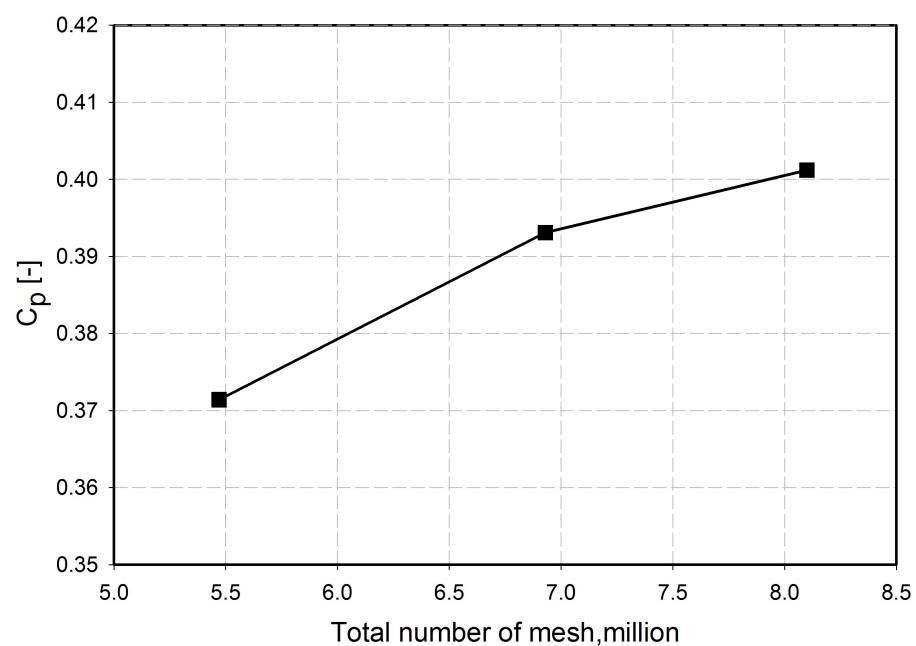


Figure 7. Effect of grid resolution on the calculated C_p for the balanced rotor.

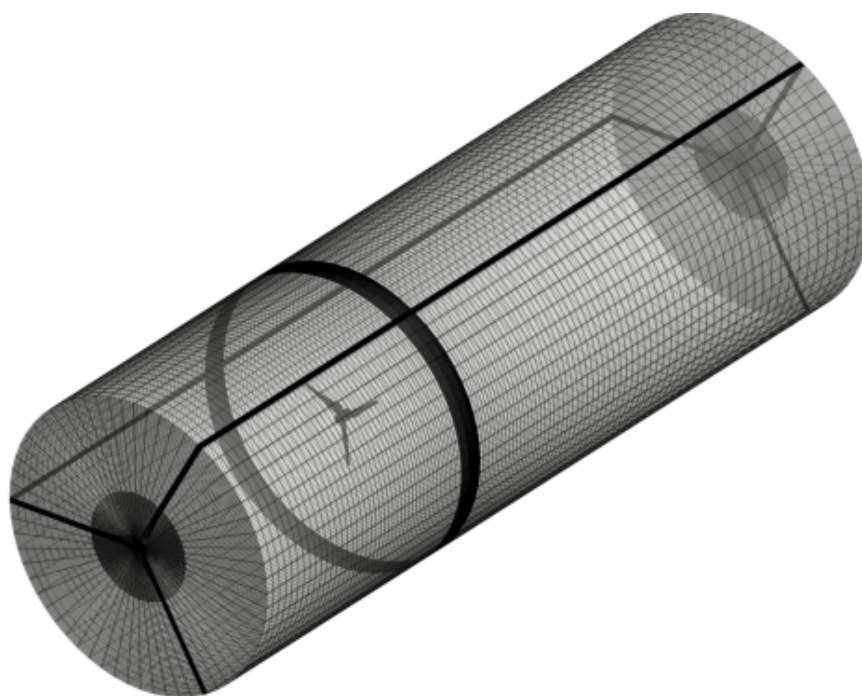


Figure 8. Computational mesh used in the present simulations.

The velocity of the incoming flow was imposed at the inlet boundary as $U_{\text{ref}} = 5.4$ m/s, with a turbulence intensity of 1%. The non-slip boundary condition was considered at the walls. A von Neumann outflow condition was applied at the outlet boundary, where a zero static pressure condition was also imposed. The computational time step is set to 0.00023, which is equivalent to 2° of turbine rotation. The number of iterations per time step is 30. The residuals of all variables are mainly below 10^{-5} except for the continuity equation which was about 10^{-4} . All simulations were performed on an HP Z800 (Intel Xeon CPU X5650, 2.66 GHz, 2 processors) workstation with 24 cores available for parallel calculations and 32 GB RAM.

In order to compare the numerical results with the experiments, single-point statistics were performed. However, the streamwise velocity variance was estimated as

$$\overline{u'^2} \approx \overline{(U - \bar{U})^2} + \frac{2}{3}k, \quad (1)$$

where the overline indicates the time-average operator. The first term is the variance of the resolved streamwise velocity in the URANS equations and corresponds to a periodic mean-flow variation not due to turbulence. The second part is obtained by assuming isotropic turbulence and that the three velocity variances composing the turbulent kinetic energy, k , were equal. The summation in Equation (1) is correct as long as the turbulent field and the mean field are uncorrelated, an hypothesis that is acceptable with the present level of approximation.

Three different studies were performed. One with a balanced rotor, one with a pitch imbalance of $+5^\circ$ replicating the experimental results and one with a pitch imbalance of -5° : the latter test will differ from the experimental conditions, but it will show if the pitch-imbalance sensitivity is symmetric or not.

4. Results

Measurements of the wake characteristics were performed downstream of the rotor at an axial distance of $x/D = 1$ and $x/D = 3$. In addition to these two planes, an additional longitudinal plane was characterised, but the statistical results did not show noticeable differences and only some spectra will be shown at specific points in this plane to illustrate the streamwise evolution of the wake dynamics. The flow field was analysed mostly in terms of the mean streamwise velocity component and its standard deviation, $\sigma_u = \overline{u'^2}^{1/2}$. All the velocity statistics were normalised with the undisturbed incoming wind-speed velocity, U_{ref} .

Figure 9 shows the mean velocity distribution in the two normal planes for both balanced and unbalanced case. While the wake velocity deficit decays in both cases, the structure of the wake remains almost axisymmetric, although the footprint of the tower presence is noticeable.

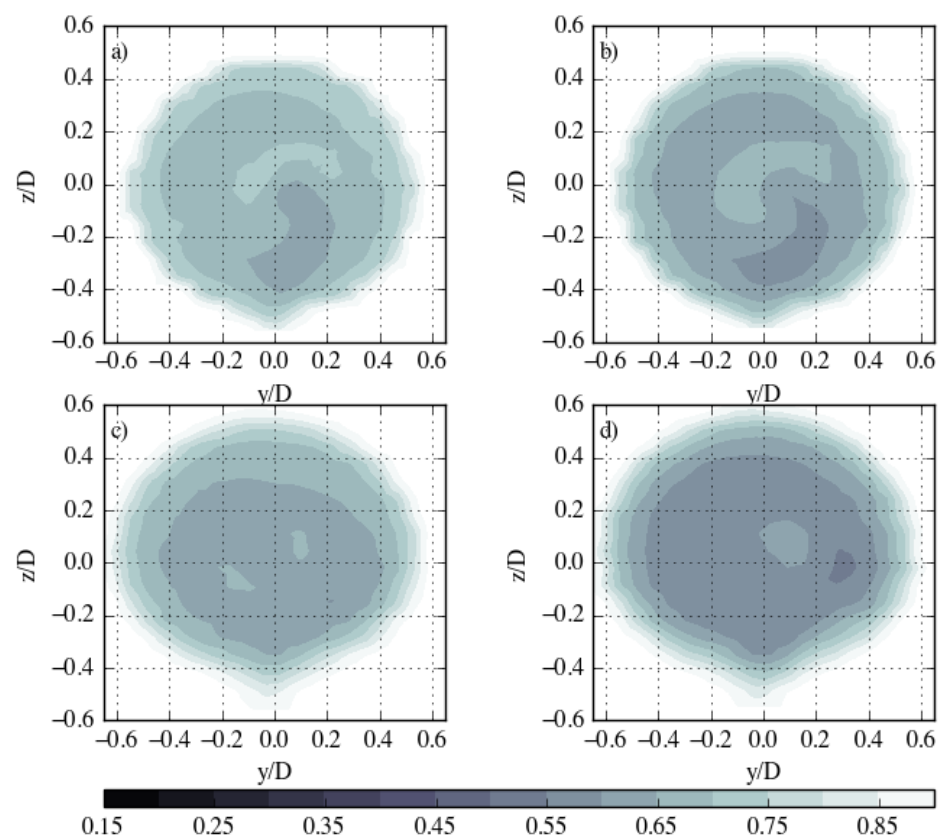


Figure 9. Experimental mean axial velocity at $x/D = 1$ (a,b) and $x/D = 3$ (c,d) for the balanced rotor (left column) and $+5^\circ$ unbalanced rotor (right column).

Similar considerations can be mentioned from the analysis of Figure 10 that illustrates the numerical results of the mean velocity at the same planes. Since the tower was not simulated, the mean velocity field is almost axisymmetric with the exception of some convergence ripples.

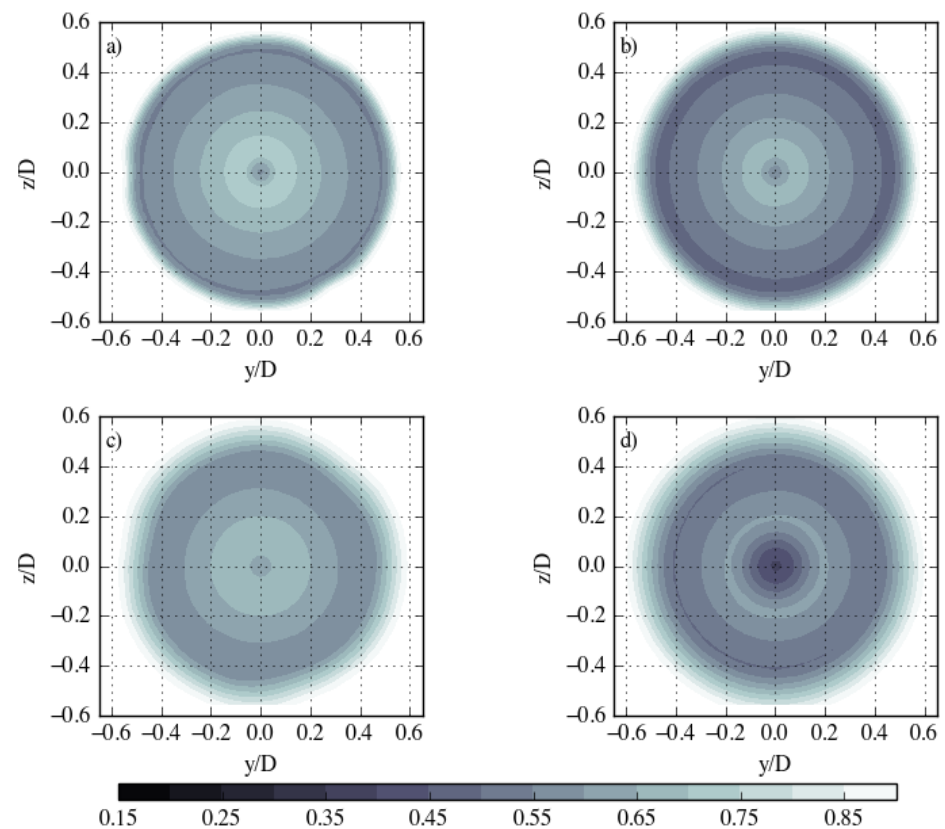


Figure 10. Numerical mean axial velocity at $x/D = 1$ (a,b) and $x/D = 3$ (c,d) for the balanced rotor (left column) and $+5^\circ$ unbalanced rotor (right column).

Much more quantitative insight can be gained by looking at the mean velocity deficit distribution at hub height, reported in Figures 11 and 12 for $x/D = 1$ and $x/D = 3$, respectively. The results of the experiments of Krogstad and Eriksen [10] are also reported as a comparison, although one should remember that the latter are affected by a larger tunnel-blockage effect, have a different tower than the present experiments and were obtained at a larger Reynolds number. It is interesting to note that the balanced case is qualitatively consistent with the results of Krogstad and Eriksen [10], although the velocity deficit is lower in the present experimental results. Both simulations and experiments point out that a positive pitch imbalance is associated with a larger wake deficit. This is not true regardless of the pitch imbalance direction: in fact, the numerical simulations with the negative pitch change show a decrease in the wake deficit as a consequence of a reduced load imparted by the blade to the flow. This is consistently observed at both $x/D = 1$ and $x/D = 3$. It is possible to note that, while at $x/D = 1$ all experimental and numerical results agree on the wake size regardless of the pitch imbalance, at $x/D = 3$ the wake expanded more in the presence of a positive pitch imbalance as a result of an increased turbulent activity rather than the natural wake expansion due to the rotor (as that should have been already completed at $x/D = 1$).

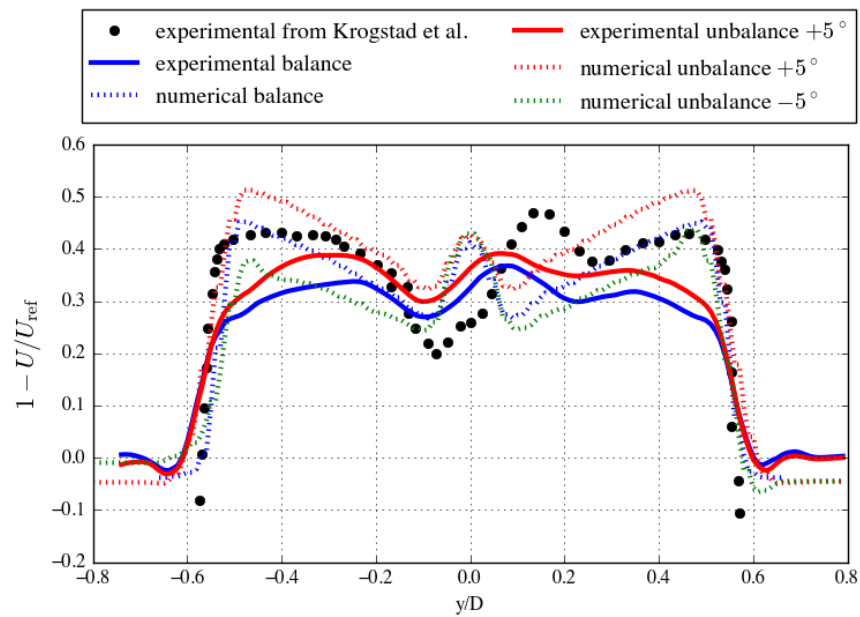


Figure 11. Numerical (dotted line) and experimental (solid line) profiles of the normalised velocity deficit at hub height for the balanced (blue lines) and unbalanced (red lines) cases at $x/D = 1$. The black circles are measurements from Krogstad and Eriksen [10]. (Green dotted lines) numerical simulations with negative pitch imbalance.

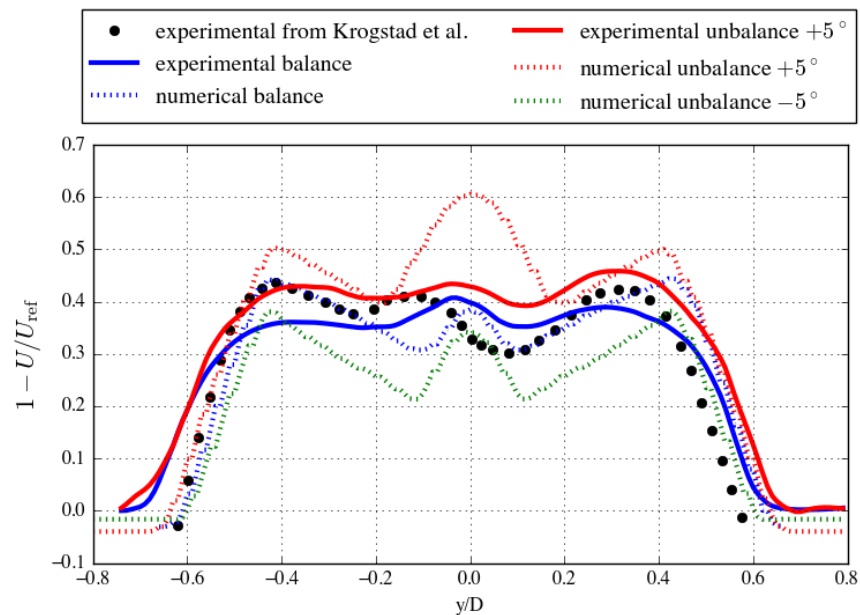


Figure 12. Numerical and experimental profiles of the normalised velocity deficit at hub height for the balanced and unbalanced cases at $x/D = 3$. See Figure 11 for the list of symbols.

Since the pitch imbalance leads to an additional fluctuating load on the blade, a greater effect is expected to be observed in the velocity fluctuation statistics. The map of the normalised velocity standard deviation measured in the experimental campaign is shown in Figure 13. The effect of the tower on the right and the bottom side of the map is clear both in the balanced and unbalanced conditions. Generally, the pitch imbalance corresponds to an increased turbulent activity, but the region behind the tower is too influenced by that to lead to some conclusion. Nevertheless, the region near the top-tip of the wake is less influenced by the tower and it clearly shows an enhanced fluctuating activity in the unbalanced case, as expected, extending more along the radial direction.

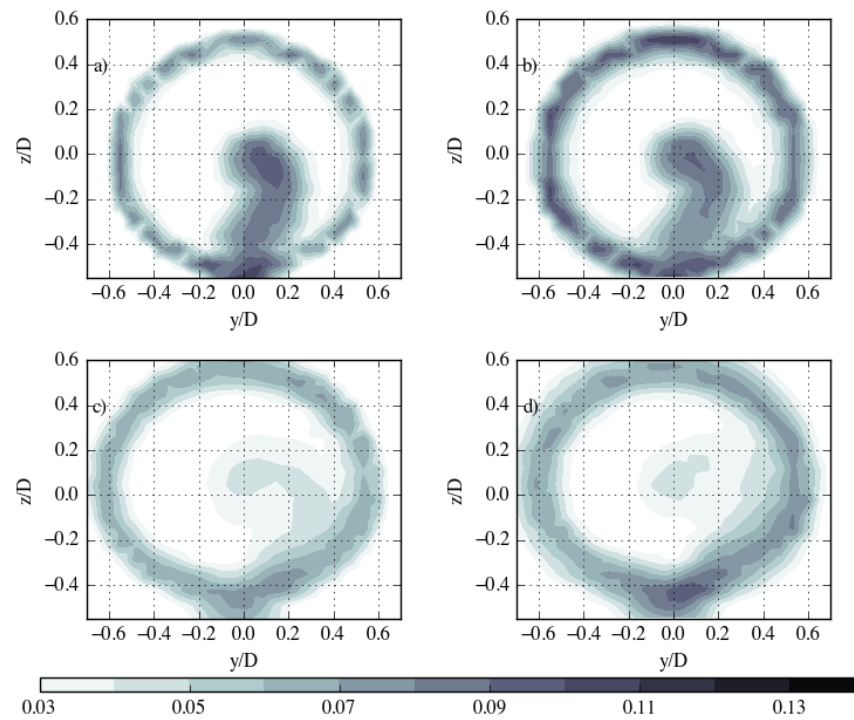


Figure 13. Experimental maps of the normalised streamwise velocity standard deviation at $x/D = 1$ (a,b) and $x/D = 3$ (c,d) for the balanced rotor (left column) and $+5^\circ$ unbalanced rotor (right column).

Figure 14 shows the velocity standard deviation determined from the numerical simulations estimated according to Equation (1). Similarly to the mean flow, the fluctuating field has also axisymmetric statistics and the magnitude of the fluctuations is enhanced in the unbalanced case, with a comparable value as in the experiments.

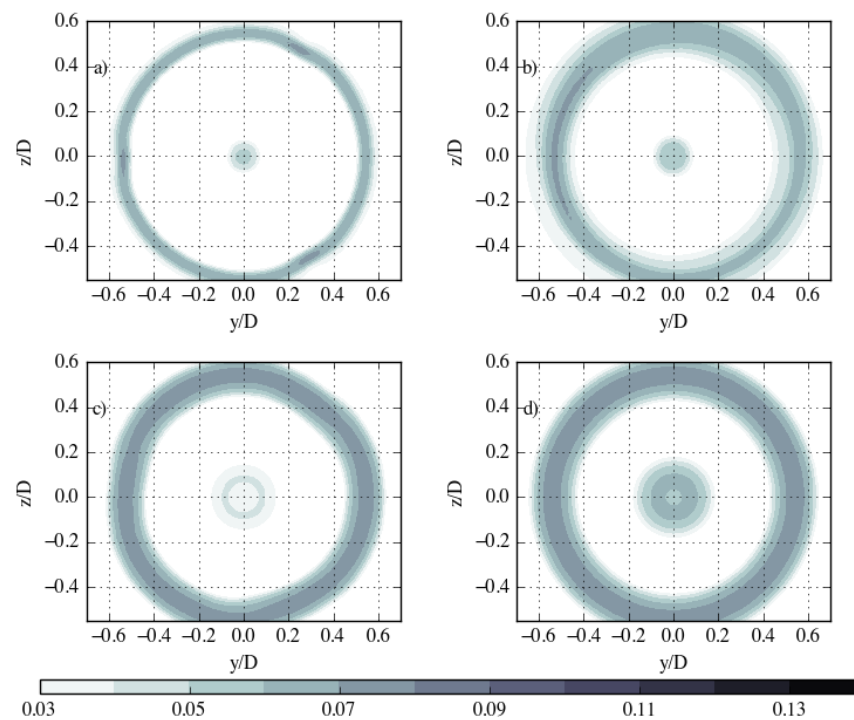


Figure 14. Numerical maps of normalised streamwise velocity standard deviation at $x/D = 1$ (a,b) and $x/D = 3$ (c,d) for the balanced rotor (left column) and $+5^\circ$ unbalanced rotor (right column).

A quantification of the unbalance effects can be achieved by looking at the hub height plane, reported in Figures 15 and 16 for $x/D = 1$ and $x/D = 3$, respectively. Krogstad and Eriksen [10] reported directly the turbulent kinetic energy, k , as a combination of the three variances: in order to compare with the present results, the turbulent kinetic energy reported by Krogstad and Eriksen [10] was multiplied by 2/3 (assuming that the variances were similar in magnitude) and the square root of that was taken, although this is not a reliable estimate since the base flow is most likely not isotropic. The standard deviation at the wake edge measured by Krogstad and Eriksen [10] is twice of the present results and this discrepancy might be due to the approximations adopted to get the streamwise standard deviation, or from the systematic differences from the present experimental setup.

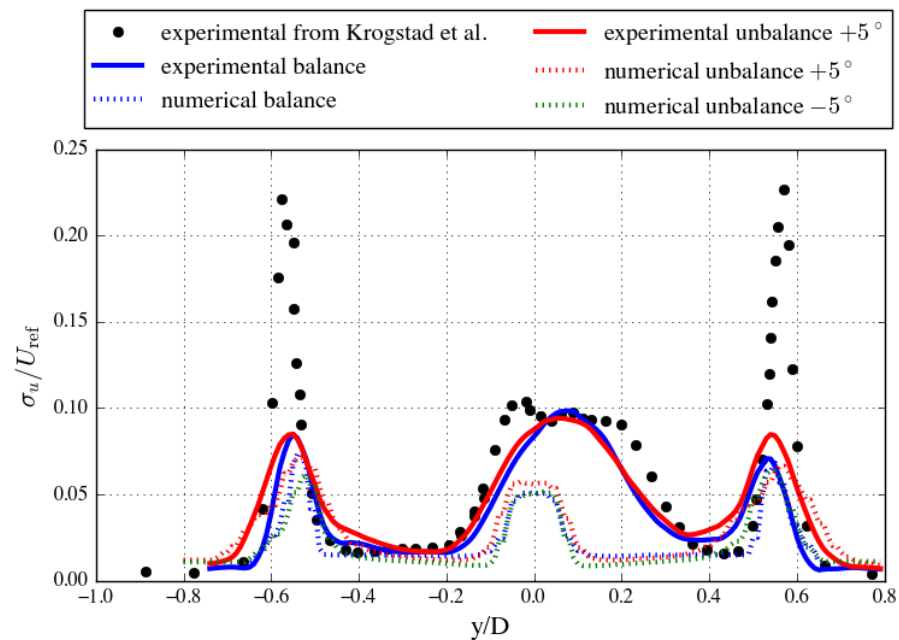


Figure 15. Numerical and experimental profiles of the normalised velocity standard deviation at hub height for the balanced and unbalanced cases at $x/D = 1$. See Figure 11 for the list of symbols.

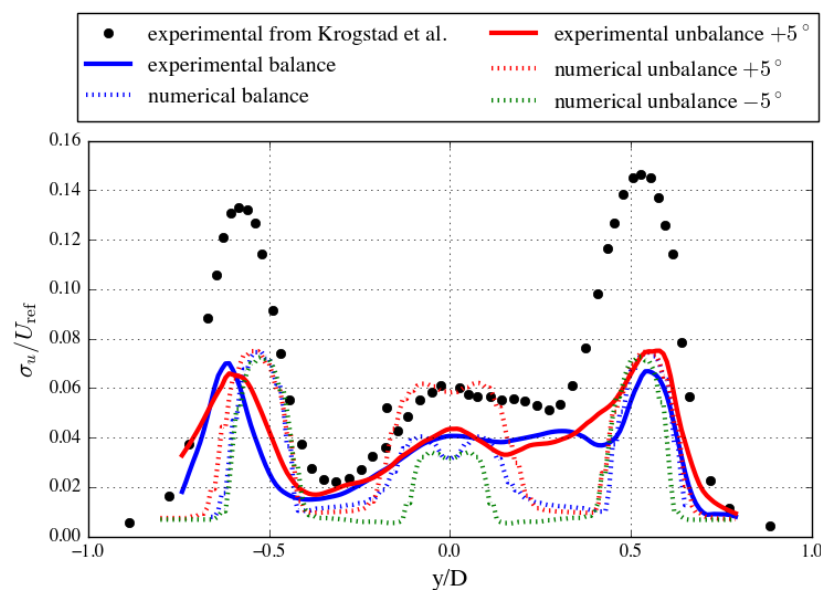


Figure 16. Numerical and experimental profiles of the normalised velocity standard deviation at hub height for the balanced and unbalanced cases at $x/D = 3$. See Figure 11 for the list of symbols.

More dynamical insight can be obtained by looking at the velocity spectra in Figure 17, showing how the fluctuating energy is distributed amongst the various frequencies. The balanced case is dominated by the tip-vortices [22] until $2D$ downstream of the rotor and their energy is redistributed at various multiple frequencies through non-linear interactions. The scenario is totally different in the unbalanced case, where there is a dominance of the rotor frequency, excited by the slight pitch imbalance. The tip vortices do not have anymore a clear signature and are most likely disorganised at an early stage as the helical vortex released by the unbalanced blade has a different convection velocity with respect to the other two. This leads to an accelerated interaction of the vortices and to the disorganisation of the wake structure present in the balanced case.

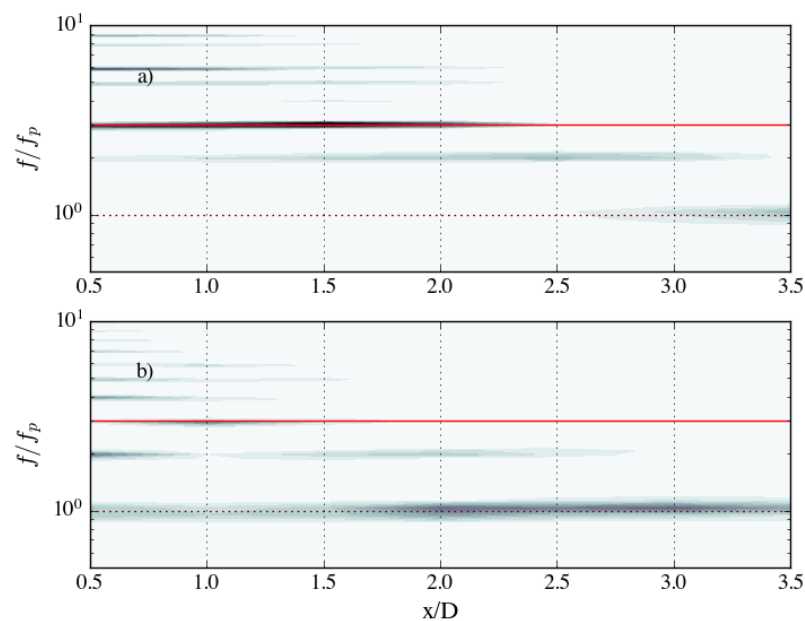


Figure 17. Pre-multiplied spectra of the experimental axial velocity, $fP_u(f)/\sigma_u^2$, at $y/D = 0$ and along $z/D = 0$ for the balanced rotor (a) and unbalanced rotor (b). The frequency is normalised by the rotation frequency of the rotor: (dotted red line) rotor frequency, (solid red line) blade passage frequency.

Further analysis about the effect of unbalancing (negative and positive 5 degree) one blade on the power and thrust coefficients of the wind turbine model was done numerically. The calculated power coefficient for positive pitch was increased by about 2.2% compared to the reference balanced turbine, and the thrust coefficient increased by 15% with respect to the balanced one. In the case of negative pitch a decrease of the power coefficient of 18% was observed together with a decrease of the thrust coefficient of 14%, in agreement with the trend of the velocity deficit observed in Figure 11. The results from negative pitch agree well with the results of Oggiano et al. [9].

The main objective of this study is to investigate the effect of unbalancing one blade on the HAWT performance and on its wake. Since the generated power from the wind turbine is mainly function of the pressure distribution along the turbine blade, the calculated static pressure coefficient on the turbine blade at $r/R = 80\%$ is presented in Figure 18 for the balanced and unbalanced case. The calculated pressure is represented in dimensionless form by using the static pressure coefficient, C_p , which is defined as

$$C_p = \frac{P - P_\infty}{1/2 \rho (U^2 + \Omega^2 r^2)}, \quad (2)$$

where P_∞ is the pressure at inlet boundary, Ω is the rotational speed of the rotor, U is the axial velocity seen by each profile, ρ is the air density and r is radius position of each section. Figure 18a–c illustrates that the pressure difference between the pressure and

suction sides of the turbine blade is generally higher at the rotor leading edge and this difference decreases towards to blade trailing edge. Therefore, most of the generated power comes from the external portion of the wind-turbine rotor. In addition to that, there is a large difference in pressure between the unbalanced blade (blade 1) and the reference one, while the pressure for blade 2 and 3 are almost identical between the balanced and unbalanced case.

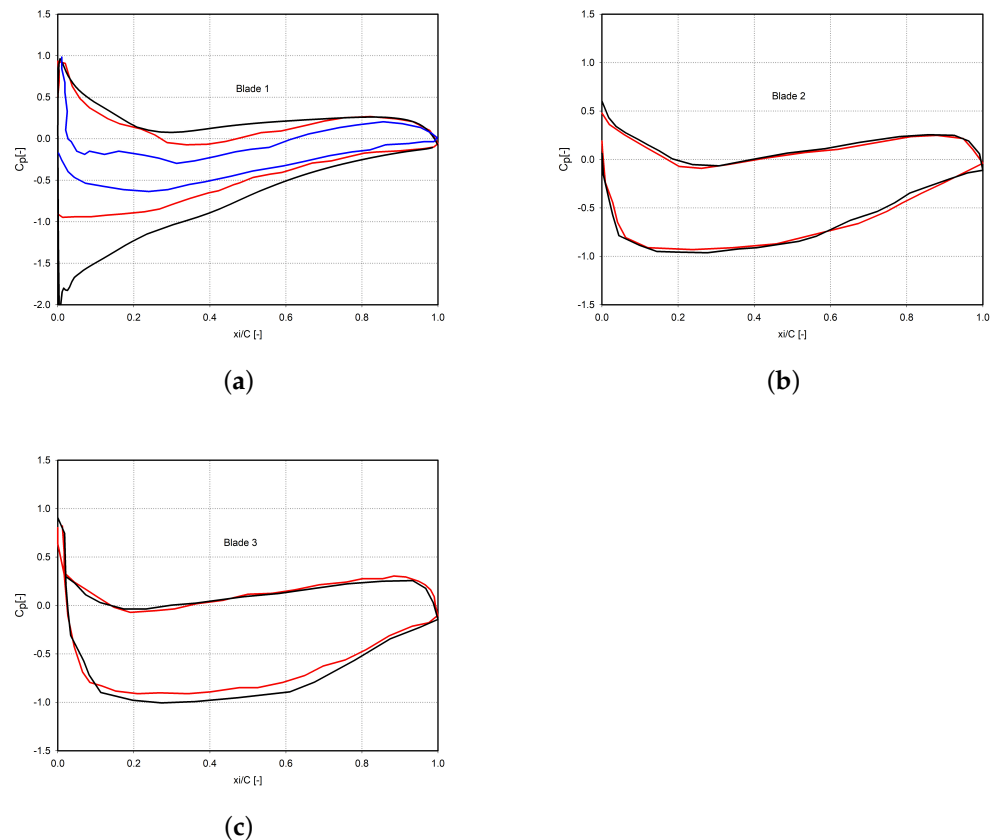


Figure 18. (a–c) Calculated static pressure coefficient at $r/R = 0.8$ for the balanced (red lines), positive pitch imbalance (black lines) and negative pitch imbalance (blue line) cases.

5. Conclusions

A comparison between a wind turbine with balanced blades (i.e., where all blades had the same pitch) and with an unbalanced blade was performed experimentally and numerically. The blade pitch was purposefully changed by 5° in one blade only to introduce a weak disturbance in the near wake that was meant to trigger the instability of the tip-vortex structure. A sensitivity study was performed numerically by unbalancing the blade by -5° , i.e., in the opposite direction. No significant effect was expected on the mean velocity deficit (in light of the small change in pitch), although the wake velocity deficit increased consistently in the (positively) unbalanced case, and the negatively unbalanced blade showed a reduced wake deficit. This suggests that the loading on the blade is enhanced by increasing the pitch angle.

A weak increase in the turbulence activity was observed for the unbalanced case regardless of the pitch-unbalance direction. This means that pitch unbalance could be used, for instance, to promote the wake recovery due to a higher turbulence activity in the wake. However, the assessment of the pitch-imbalance effect in the far wake was not possible here since the traversing did not allow us to characterise the wake at distances larger than $3D$.

From Figure 17 it is noticeable that the larger velocity fluctuation is associated with a different evolution of the frequency spectra: while the balanced case is dominated by the tip-vortex frequency (i.e., the blade-passage frequency), the unbalanced case is dominated by the rotor frequency and the tip-vortex peak disappeared before $1D$, suggesting that the pitch imbalance promotes the disorganisation of the wake structure by altering the convection velocity of the tip spirals, leading to a faster vortex interaction and coalescence.

According to the present numerical results, a sensible decrease of the power coefficient has been observed together with an increase/decrease of the thrust coefficient, depending on the imbalance direction, as the blade operates then in off-design conditions. Remarkably, only the blade affected by the pitch imbalance is subjected to a modification of the aerodynamic loads (as is visible from the pressure coefficient distribution), while the other blades do not alter their loads and do not suffer from increased fatigue loads.

Author Contributions: Conceptualization, A.S. and F.C.; methodology, M.B.; software, M.B.; investigation, A.E., A.S. and F.C.; resources, A.S. and F.C.; data curation, A.S.; writing—original draft preparation, F.C., A.S. and A.E.; writing—review and editing, F.C., A.S., M.B. and A.E. All authors have read and agreed to the published version of the manuscript

Funding: This research received no external funding.

Institutional Review Board Statement: Not Applicable.

Informed Consent Statement: Not Applicable.

Data Availability Statement: Not Applicable.

Conflicts of Interest: The authors declare no conflict of interest.

References

1. Astolfi, D. A study of the impact of pitch misalignment on wind turbine performance. *Machines* **2019**, *7*, 8. [[CrossRef](#)]
2. Aramendia, I.; Fernandez-Gamiz, U.; Zulueta, E.; Saenz-Aguirre, A.; Teso-Fz-Betoño, D. Parametric study of a gurney flap implementation in a du91w (2) 250 airfoil. *Energies* **2019**, *12*, 294. [[CrossRef](#)]
3. Jing, B.; Qian, Z.; Pei, Y.; Zhang, L.; Yang, T. Improving wind turbine efficiency through detection and calibration of yaw misalignment. *Renew. Energy* **2020**, *160*, 1217–1227. [[CrossRef](#)]
4. Astolfi, D.; Castellani, F.; Becchetti, M.; Lombardi, A.; Terzi, L. Wind Turbine Systematic Yaw Error: Operation Data Analysis Techniques for Detecting It and Assessing Its Performance Impact. *Energies* **2020**, *13*, 2351. [[CrossRef](#)]
5. Castellani, F.; Astolfi, D.; Natili, F.; Mari, F. The yawing behavior of horizontal-axis wind turbines: A numerical and experimental analysis. *Machines* **2019**, *7*, 15. [[CrossRef](#)]
6. Bossanyi, E.A. Individual Blade Pitch Control for Load Reduction. *Wind Energy* **2003**, *6*, 119–128. [[CrossRef](#)]
7. Kanev, S.K.; van Engelen, T.G. Exploring the Limits in Individual Pitch Control. In Proceedings of the European Wind Energy Conference and Exhibition, Marseille, France, 16–19 March 2009; pp. 679–704.
8. Namik, H.; Stol, K. Individual blade pitch control of floating offshore wind turbines. *Wind Energy* **2010**, *13*, 74–85. [[CrossRef](#)]
9. Oggiano, L.; Boorsma, K.; Schepers, G.; Kloosterman, M. Comparison of simulations on the NewMexico rotor operating in pitch fault conditions. *J. Phys. Conf. Ser.* **2016**, *753*, 022049. [[CrossRef](#)]
10. Krogstad, P.Å.; Eriksen, P.E. “Blind test” calculations of the performance and wake development for a model wind turbine. *Renew. Energy* **2013**, *50*, 325–333. [[CrossRef](#)]
11. Segalini, A.; Inghels, P. Confinement effects in wind-turbine and propeller measurements. *J. Fluid Mech.* **2014**, *756*, 110–129. [[CrossRef](#)]
12. Fluent, A. *Fluent 14.0 User's Guide*; ANSYS FLUENT Inc.: Las Vegas, NV, USA, 2011.
13. Bardina, J.E.; Huang, P.G.; Coakley, T.J. Turbulence modeling validation, testing, and development. In Proceedings of the 28th Fluid Dynamics Conference, Snowmass Village, CO, USA, 29 June–2 July 1997; p. 2121.
14. Menter, F.R. Two-equation eddy-viscosity turbulence models for engineering applications. *AIAA J.* **1994**, *32*, 1598–1605. [[CrossRef](#)]
15. Hsiao, F.B.; Bai, C.J.; Chong, W.T. The performance test of three different horizontal axis wind turbine (HAWT) blade shapes using experimental and numerical methods. *Energies* **2013**, *6*, 2784–2803. [[CrossRef](#)]
16. Burlando, M.; Ricci, A.; Freda, A.; Repetto, M.P. Numerical and experimental methods to investigate the behaviour of vertical-axis wind turbines with stators. *J. Wind. Eng. Ind. Aerodyn.* **2015**, *144*, 125–133. [[CrossRef](#)]
17. Lee, M.H.; Shiah, Y.C.; Bai, C.J. Experiments and numerical simulations of the rotor-blade performance for a small-scale horizontal axis wind turbine. *J. Wind. Eng. Ind. Aerodyn.* **2016**, *149*, 17–29. [[CrossRef](#)]
18. Fluent, I. *Gambit 2.4 Tutorial Guide*; FLUENT Inc.: Lebanon, NH, USA, 2007.

19. Van Rooij, R.; Arens, E. Analysis of the experimental and computational flow characteristics with respect to the augmented lift phenomenon caused by blade rotation. *J. Phys. Conf. Ser.* **2007**, *75*, 1742–6596.
20. Moshfeghi, M.; Song, Y.J.; Xie, Y.H. Effects of near-wall grid spacing on SST-K- ω model using NREL Phase VI horizontal axis wind turbine. *J. Wind. Eng. Ind. Aerodyn.* **2012**, *107*, 94–105. [[CrossRef](#)]
21. Eltayesh, A.; Hanna, M.B.; Castellani, F.; Huzayyin, A.; El-Batsh, H.M.; Burlando, M.; Becchetti, M. Effect of wind tunnel blockage on the performance of a horizontal axis wind turbine with different blade number. *Energies* **2019**, *12*, 1988. [[CrossRef](#)]
22. Segalini, A.; Alfredsson, P.H. A simplified vortex model of propeller and wind-turbine wakes. *J. Fluid Mech.* **2013**, *725*, 91–116. [[CrossRef](#)]